KSME

Springer

Journal of Mechanical Science and Technology 37 (1) 2023

Original Article
DOI 10.1007/s12206-022-1223-2

Keywords:
· GRNN
· Multi-constraint
· Optimization design
· Small sample
· Wind turbine airfoils

Correspondence to:
Xudong Wang
wangxudong916@163.com

Citation:
Wang, X., Ju, H., Lu, J. (2023). Wind turbine airfoils optimization design by generalized regression neural network under small sample. Journal of Mechanical Science and Technology 37 (1) (2023) 217~228. http://doi.org/10.1007/s12206-022-1223-2

Received March 27th, 2022
Revised August 28th, 2022
Accepted September 22nd, 2022

† Recommended by Editor Hyun-Gyu Kim

Wind turbine airfoils optimization design by generalized regression neural network under small sample

Xudong Wang, Hao Ju and Jiahong Lu

Chongqing Key Laboratory of Manufacturing Equipment Mechanism Design and Control, Chongqing Technology and Business University, Chongqing 400067, China

Abstract Neural network models can quickly and accurately predict the aerodynamic performance of wind turbine airfoils based on existing data, but the construction of a large number of learning samples requires a high upfront time cost. To address this problem, a generalized regression neural network (GRNN) model of wind turbine airfoils based on a small sample set is established, and an optimal design method for airfoil aerodynamic performance under multiple constraints is proposed. This method is used to improve the prediction accuracy of the model in the optimization process and to solve the problem of insufficient learning caused by poor training data. Based on the established optimal design model, we applied the particle swarm optimization (PSO) algorithm to complete the optimal design of NACA44XX series airfoils and obtained the optimized airfoils with maximum relative thicknesses of 15 %, 18 %, 21 %, and 24 %, respectively. The aerodynamic characteristics of the new airfoils were analyzed in comparison with the baseline airfoils. The results show that the aerodynamic properties of the new airfoils are significantly improved, with the maximum lift coefficient and maximum lift-to-drag ratio increasing by up to 16.93 % and 10.41 %. Moreover, the optimization efficiency of the method is much higher than that of the traditional one. Thus, it was verified that the method is feasible and effective.

1. Introduction

The airfoil is the basic element that makes up the blade, and its design and optimization require solving complex high-dimensional nonlinear hydrodynamic problems. Computational fluid dynamics (CFD) method has become the main tool for aerodynamic design at this stage with its high accuracy and confidence [1, 2]. However, its computational cycle is long and usually consumes huge computer computing power.

In recent years, machine learning and neural network technologies have developed significantly, and data-driven modeling methods tend to be popular. Therefore, some scholars have applied them to flow field prediction and airfoil optimization design. Zhu et al. [3] developed a direct construction of a purely data-driven algebraic model of turbulence through radial basis function neural networks, which successfully realized the coupled solution between the model and the N-S equations, opening the way for artificial intelligence methods to solve engineering turbulence problems. Oztiryaki et al. [4] simplified the prediction of lift coefficients using shallow neural networks and utilized them for dynamic optimization design. Kutz [5] and Ling [6] constructed a tensor-based neural network model of Reynolds stress anisotropy to portray the vortex structure in secondary flows and separation phenomena in wave walls. Zahn [7] proposed a nonlinear system reduced-order modeling technology based on long and short time memory neural network, which was used to predict the aerodynamics of transonic chattering. Balla [8] established a multi-output neural network by taking the pressure of airfoil fixed points as the output. Compared with the orthogonal decomposition method, this method can achieve higher precision prediction. Deng et al. [9] proposed a vortex intelligent extraction algorithm

based on a convolutional neural network, which has a low false-positive rate and balances performance and accuracy well. Sekar et al. [10] proposed a deep neural network method for the rapid prediction of airfoil flow field. A mapping model with airfoil parameters, Reynolds number, and angle of attack as input and flow field distribution as output was constructed. This method has high computational efficiency and generalization ability for different airfoil profiles.

These studies show the great potential of neural networks in dealing with high-dimensional nonlinear hydrodynamics problems, but also confirm that the performance of their models depends heavily on learning samples. However, obtaining a large number of high-precision samples requires high time cost, and less training data will lead to inadequate network learning.

Generalized regression neural network (GRNN) provides a feasible idea for the solution of this problem. Compared with other neural networks, GRNN has stronger nonlinear mapping ability and faster learning speed, which can achieve accurate prediction under a small sample set. Lyu et al. [11] used generalized regression neural network to predict the aerodynamic coefficients of rotor blades. With the training of a small number of samples, the lift coefficient, drag coefficient and torque coefficient of the airfoil were accurately predicted with shape parameters and flow conditions as inputs, which greatly saved the time of constructing a complex sample database. Sun et al. [12] compared the prediction values of BP (back propagation, BP) neural network, RBF (radial basis function, RBF) neural network and GRNN neural network for airfoil aerodynamic parameters with the same number of samples. The analysis results show that the predicted values of GRNN are more accurate.

In the optimization design process, the situation is more complicated. Wang et al. [13] established the inverse design model of airfoil lift robustness based on GRNN, and output the airfoil shape that meets the requirements with lift value as the design target. The data dimension is reduced by principal component analysis (PCA) to reduce the number of database samples. Kharal and Saleem [14] described the airfoils by Bezier-Parsec parameterization method, used GRNN to predict the shape parameters of the optimal airfoils under a given pressure coefficient distribution, and combined with genetic algorithm to successfully achieve the optimal design of two kinds of original airfoils. However, the above optimization design is to solve nonlinear problems with uncertain boundaries, and its well-posedness problem is complex and depends heavily on the experience of designers [15].

In contrast, the direct numerical optimization method of airfoil shapes is more intuitive and simple. The extreme values of the objective functions (such as maximum lift coefficient and maximum lift-drag ratio) are sought by continuously modifying the airfoil shape to obtain and compare intermediate airfoils, and the optimal airfoil shape is finally obtained [16]. However, during direct numerical optimization, a large amount of noisy data usually appears, which has a huge impact on the prediction accuracy of neural networks [17]. In particular, neural network prediction models based on small sample sets are not sufficiently learned because of their small training sets. The neural network model prediction is more accurate when the input conforms to the pattern of the sample database data; conversely, when the input does not meet the pattern of the sample database data, it produces a large error. In the optimization process, the variation of the neural network input is usually random, so a considerable part of noisy data will be input into the neural network model, which is prone to misjudgment and thus interferes with the whole optimization process.

In view of this problem and combined with the practice of airfoil design, this paper proposes to use multi-constraint conditions to limit the input variables of neural network to make them meet certain rules, so as to improve the prediction accuracy and solve the problem of insufficient learning caused by training based on small sample sets. Furthermore, it is combined with particle swarm optimization algorithm for direct numerical optimization to obtain better performance of wind turbine airfoil series.

2. Modeling of airfoils by GRNN

2.1 GRNN model

Generalized regression neural network is a kind of radial basis function neural network. It is based on non-parametric kernel regression and takes sample data as a posteriori condition to solve the connection probability density function between independent variables and dependent variables by observation samples, so as to calculate the regression value of the latter to the former [18]. GRNN consists of the following four layers.

(1) Input layer: The number of neurons in the input layer is equal to the dimensions of the input vector, which is transmitted to the mode layer without any transformation.

(2) Pattern layer: Each neuron corresponds to the training sample individually, with Gaussian function as the activation kernel function, and the input vector is transformed in the mode layer as follows.

$$P_i = \mathrm{e}^{\left[-\frac{(X-X_i)^{\mathrm{T}}(X-X_i)}{2\sigma^2}\right]} \quad i=1,2,...,n \tag{1}$$

Where, X is the network input vector; Xi is the learning sample corresponding to the i-th neuron; σ is a smooth factor.

(3) Summation layer: This layer contains two types of summation neurons, one of which sums all outputs of the pattern layer arithmetically. The connection weight of each neuron in the pattern layer is 1, and the transfer function is as follows.

$$S_{\mathrm{D}} = \sum_{i=1}^{n} P_i \tag{2}$$

In the other category, all outputs of the pattern layer are weighted summation. The connection weight between the neuron of the i-th pattern layer and neuron of the j-th summation

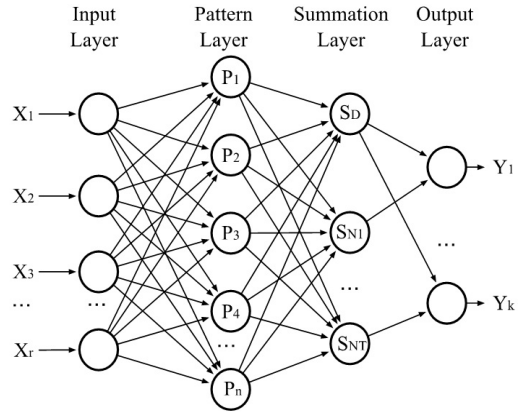

Fig. 1. The structure of GRNN.

layer is the j-th element in the output sample Yi of the i-th.

$$S_{Nj} = \sum_{i=1}^{n} y_{ij} P_i \quad j = 1,2,...,k \tag{3}$$

(4) Output layer: The output of the j-th neuron corresponds to the j-th element of the predicted result Y(X).

$$y_i = \frac{S_{Nj}}{S_D} \quad j = 1,2,...,k \tag{4}$$

The basic structure of GRNN is shown in Fig. 1.

2.2 Construction of airfoil sample database

The performance of neural network depends heavily on learning samples. For airfoil design, sample database should cover a wide range of shape changes. The NACA four-digit airfoil series is the first low-speed airfoil series with high lift and low drag established in the U.S. The airfoil can be accurately described by three shape parameters: T_{max}, C_{max}, and x_C [19]. The equations are as follows (assuming chord is 1).

$$y_c = \begin{cases} \dfrac{C_{\max}(2x_C x - x^2)}{x_C^{\,2}} & 0 \le x \le x_C \\ \dfrac{C_{\max}(1 - 2x_C + 2x_C x - x^2)}{(1 - x_C)^2} & x_C \le x \le c \end{cases} \tag{5}$$

$$y_t = \frac{T_{\max}}{0.2}\left(\begin{array}{l} 0.2969x^{0.5} - 0.1260x - 0.3516x^2 + \\ 0.2843x^3 - 0.1015x^4 \end{array}\right) \tag{6}$$

$$\begin{cases} x_{\text{upper}} = x - y_t \sin\left(\arctan\left(\dfrac{\mathrm{d}y_c}{\mathrm{d}x}\right)\right) \\ y_{\text{upper}} = y_c + y_t \cos\left(\arctan\left(\dfrac{\mathrm{d}y_c}{\mathrm{d}x}\right)\right) \\ x_{\text{lower}} = x + y_t \sin\left(\arctan\left(\dfrac{\mathrm{d}y_c}{\mathrm{d}x}\right)\right) \\ y_{\text{lower}} = y_c - y_t \cos\left(\arctan\left(\dfrac{\mathrm{d}y_c}{\mathrm{d}x}\right)\right) \end{cases} \tag{7}$$

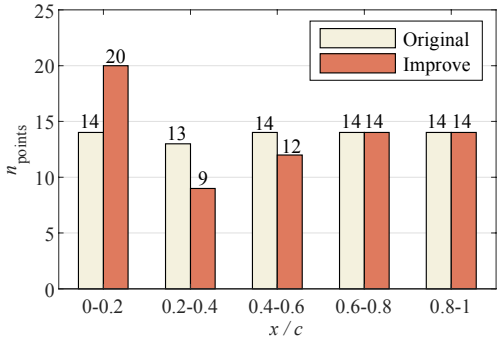

Fig. 2. Comparison of the distribution of discrete points.

Where, y_c is the coordinate of airfoil mean line, mm; y_t is half of the airfoil thickness, mm; x and y are the two-dimensional coordinates of the airfoil, mm.

The equations can be calculated to obtain the two-dimensional discrete coordinate points of the airfoil with the specified shape. However, when there are fewer discrete points, the distribution of points is more scattered and the description is not accurate at the leading edge. Therefore, this experiment proposes to add an improved equation for the distribution of airfoil points.

$$x = \begin{cases} \dfrac{\sin(\pi x - 0.5\pi) + 1}{2} & x < 0.5 \\ x & x \ge 0.5 \end{cases} \tag{8}$$

With the above transformation, the discrete points at the middle of the airfoil, where the curvature changes gently, can be brought closer to the curved leading edge while the total number of discrete points remains unchanged. Fig. 2 shows the distribution of discrete points in each segment of the chord length direction when the total number of discrete points is 69.

In this paper, the improved equation above was used to obtain the airfoil data when the three shape parameters changed uniformly in a large range, which was taken as the learning sample. The geometric parameters of NACA four-digit airfoils are defined in a larger range of reasonable airfoils as shown in Eq. (9).

$$\begin{cases} 1\% \le C_{\max} \le 6\% \\ 30\% \le x_C \le 50\% \\ 14\% \le T_{\max} \le 26\% \end{cases} \tag{9}$$

where T_{max} is taken once for every 2 % variation. The three groups of parameters were arbitrarily combined and substituted into the improved NACA four-digit airfoil equations to obtain 126 groups of airfoil coordinates as sample airfoils.

2.3 CST parameterization of airfoils

Neural networks are essentially mappings between inputs and outputs. If the airfoil discrete points are directly used as

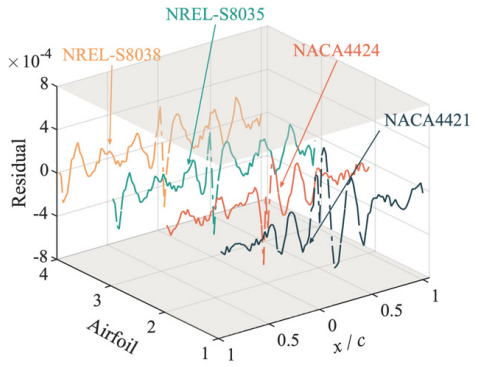

Fig. 3. Fitting residuals of the four airfoils.

input variables, it will lead to problems such as high dimensionality [20], high computational effort as well as overfitting. Therefore, airfoil parameterization is essential. Class function/shape function transformation (CST) parameterization uses a class function to control the type of airfoil represented, and the specific airfoil is uniquely determined by the coefficients of the shape function. This method has the characteristics of fewer design variables, wide design space and smooth airfoil generation [21]. Its basic formula is:

$$\begin{cases} y_{\text{upper}} = C_{N2}^{N1}(x)S(x)_{\text{upper}} + x\Delta z_{\text{upper}} \\ y_{\text{lower}} = C_{N2}^{N1}(x)S(x)_{\text{lower}} + x\Delta z_{\text{lower}} \end{cases} \tag{10}$$

$$C_{N2}^{N1}(x) = x^{N1}\cdot(1-x)^{N2} \tag{11}$$

$$S(x) = \sum_{i=0}^{n} \frac{a_i n! x^i (1-x)^{n-i}}{i!(n-i)!} \tag{12}$$

Where, x is the abscissa of airfoil points, mm; y is the ordinate of the airfoil points on the upper and lower airfoils, mm; N_1 and N_2 are the determinative coefficients of class functions. When they are 0.5 and 1 respectively, they represent the airfoil with round leading edge and sharp trailing edge. a_i is the shape function coefficient; n is the order of the shape function.

In this paper, the CST method was chosen to parameterize the airfoil. In order to satisfy the accuracy criteria and reduce the amount of coefficient variables, the upper and lower airfoils were fitted with a polynomial of the 5th order type function, and a total of 12 coefficient variables were used to parameterize the airfoil. The airfoils were all pointed trailing edge and Δz was set to 0. In order to test the accuracy of the above parameterization method, NACA4421 ($T_{\max}$ = 21 %) and NACA4424 ($T_{\max}$ = 24 %) in NACA airfoil series and S8035 ($T_{\max}$ = 17.5 %) and S8038 ($T_{\max}$ = 13 %) in NREL-S wind airfoil series were selected for fitting test, the fitting residuals are shown in Fig. 3. The values are less than 8×10^{-4}, which fulfilled the wind tunnel test demand. Therefore, the parameterization method can accurately represent the airfoils.

2.4 Training of neural network models

(1) The airfoils in the sample database were parametrized to obtain 126 sets of 12-dimensional coefficient vectors, which were normalized to [0, 1] according to the dimensions and served as the input part of the GRNN. The XFOIL program was used to quickly calculate the C_L/C_D for an airfoil located at an angle of attack of 5° under specific operating conditions (Re = 1.6×10^{-6}, Ma = 0.37), which was used as the output part of the neural network. Excluding the non-converging airfoils, a total of 124 sets of data were generated.

(2) The 124 sets of airfoil data in the sample library were divided, of which 90 % (112 sets of data) was used as the training set, and 10 % (12 sets of data) was used as the test set. In order to examine the performance of the trained neural network model more comprehensively and reliably, the selected test set of airfoils should be representative and cover the whole sample space as much as possible. However, the difference of T_{max} will lead to a large difference in the C_L/C_D of the airfoils. Therefore, stratified sampling was carried out for the whole sample library based on T_{max}. Meanwhile, over-thick or over-thin airfoils (T_{max} > 25 % or T_{max} < 15 %) need to be designed separately, and the testing in this area can be reduced appropriately.

According to the above criteria, 2 samples were randomly selected from each of the airfoils with T_{max} of 16 %, 18 %, 20 %, 22 % and 24 %, and 1 sample was randomly selected from each of the airfoils with T_{max} of 14 % and 16 %, making a total of 12 airfoils to form the test set, and the remaining airfoils were used as the training set. In this way, the sampling ratio within each stratum in the main test area is basically consistent with the overall sampling ratio, and the data bias caused by completely random sampling is avoided.

Finally, the best smoothing factor is determined by cross validation, and the generalized regression network model is established. The goodness of fit (R^2), mean square error (MSE) and mean absolute percentage error (MAPE) were used to evaluate the neural network model. The evaluation formula is as follows.

$$R^2 = \frac{\left(n\sum_{i=1}^{n}\hat{y}_i y_i - \sum_{i=1}^{n}\hat{y}_i\sum_{i=1}^{n}y_i\right)^2}{\left(n\sum_{i=1}^{n}\hat{y}_i^{\,2} - \left(\sum_{i=1}^{n}\hat{y}_i\right)^2\right)\left(n\sum_{i=1}^{n}y_i^{\,2} - \left(\sum_{i=1}^{n}y_i\right)^2\right)} \tag{13}$$

$$MSE = \frac{1}{n}\sum_{i=1}^{n}(\hat{y}_i - y_i)^2 \tag{14}$$

$$MAPE = \frac{1}{n}\sum_{i=1}^{n}\left(\left|\frac{\hat{y}_i - y_i}{y_i}\right|\right)\times100\% \tag{15}$$

The training and testing results of the neural network are shown in Fig. 4 and Table 1. The performance of the training set is satisfactory in all aspects while the MSE of the test set is relatively large due to the wide output domain and the few outliers. However, the R^2 of the test set is close to 1, the predicted value is in line with the global fitting trend, the MAPE is small, and the mean fitting degree of local individuals is high. Therefore, the neural network model has a superior predictive ability

Table 1. Performance evaluation of neural network prediction.

	Spread	Sample size	R^2	*MSE*	*MAPE*/%
Training samples	0.26	112	0.9992	0.9415	0.16
Test samples	0.26	12	0.9926	9.8771	0.19

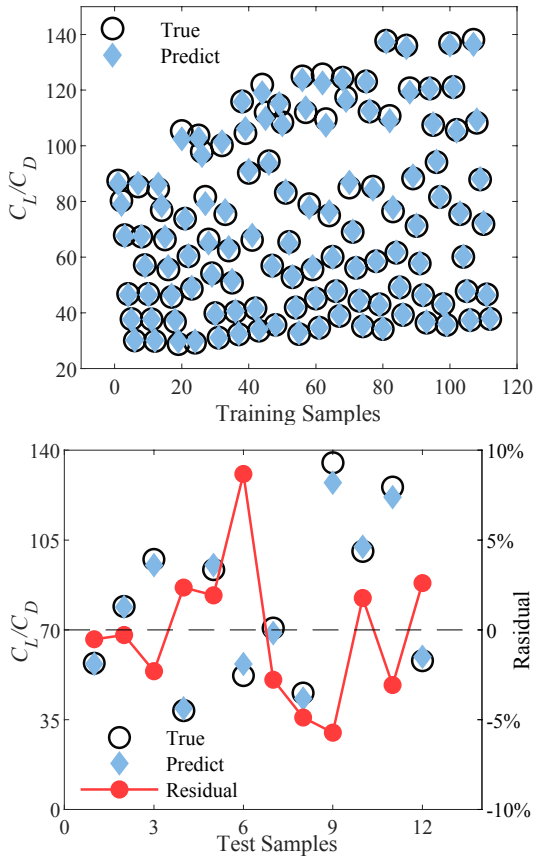

Fig. 4. Training and testing results of neural network.

as well as a strong generalization ability.

3. Airfoil optimization with multi-constraints

3.1 Limitations of direct optimization

In the optimization process, the curve composed of design variables may not conform to the airfoil characteristics and become a set of noise data. Neural networks trained on small sample sets cannot accurately predict such data, which will interfere with the whole optimization process. The constructed GRNN model combined with intelligent algorithm was used for multiple optimization designs, and the results are shown in Fig. 5. The optimized result is disturbed by noise data and has more fluctuations in the lower airfoil profile, which does not conform to the airfoil pattern and has poor actual aerodynamic performance.

In addition, further quantitative analysis of the optimization process was carried out. After CST parameterization of airfoils

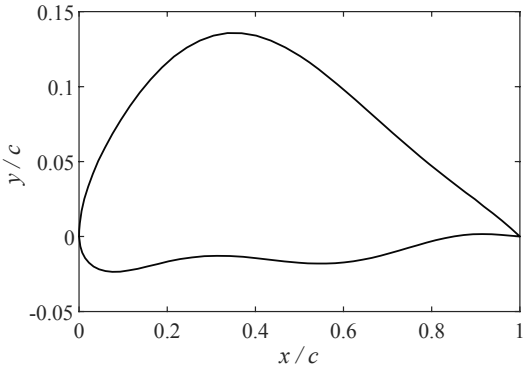

Fig. 5. Airfoil with failed optimization.

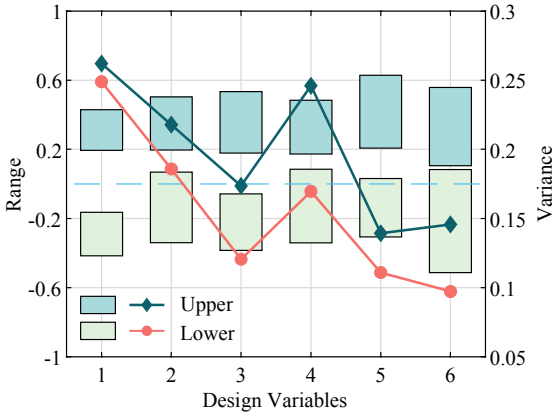

Fig. 6. Range and dispersion of coefficients.

in the sample library, the coefficient range and dispersion degree of the upper and lower airfoils are shown in Fig. 6. The dispersion degree of the coefficients is evaluated by the variance, which is calculated as shown in Eq. (16).

$$s^2 = \frac{1}{n}\sum_{i=1}^{n}(x_i - x_{ave})^2 \tag{16}$$

where, s^2 is the variance, n is the number of samples, x_i is the CST coefficients, and x_{ave} is the mean of the CST coefficients.

The analysis shows that the upper and lower airfoils correspond to 6 coefficient variables each, and the overall range of variation of the coefficient variables at the corresponding positions does not differ significantly. But in the lower airfoil, the range of variation between adjacent coefficients is more different, and there are positive and negative transformations in the values of the 2nd, 4th, 5th and 6th coefficient variable, which means that the profile of the lower airfoil is more complex. Meanwhile, the variance of each coefficient variable in the upper and lower airfoil was compared. In contrast to the upper airfoil, the variance of the lower airfoil is smaller, which means that the change in the coefficient variables of the lower airfoil is more slight. Under the training of small sample, the neural network model is not sufficiently learned, and the aerodynamic performance changes caused by the slight adjustment of coef-

ficient variables in the optimization process cannot be accurately predicted.

3.2 Presentation of multiple constraints

To avoid the limitations in direct optimization and without increasing the number of training samples, the following multiple constraints are proposed directly from the above optimization results for the design variables to shift the model input vectors towards certain laws, avoid the appearance of noisy data and deformed airfoils, and improve the prediction accuracy of the neural network.

(1) Profile constraints on concavity and convexity

The fluctuation of airfoil profile is the change of curve bending direction, which is reflected as the variation of curve convexity in function. Therefore, the second-order derivative of the airfoil expression can be used to limit the number of profile concavity transformations. For a single flank surface, the number of changes should not exceed 1. This paper deals with an airfoil with rounded leading edge and sharp trailing edge, where N_1 takes the value of 0.5, N_2 takes the value of 1, and Δz is set to 0. Eqs. (10)-(12) are used to find the first-order and second-order derivatives of x, the combination simplifies as follows.

$$y'(x)=\sum_{i=0}^{n}\left[\frac{a_i n!}{i!(n-i)!}\left[\begin{matrix}(i+0.5)x^{i-0.5}(1-x)^{n-i+1}-\\(n-i+1)x^{i+0.5}(1-x)^{n-i}\end{matrix}\right]\right] \tag{17}$$

$$y''(x)=\sum_{i=0}^{n}\left[\frac{a_i n!\left[\begin{matrix}(i^2-0.25)x^{i-1.5}(1-x)^{n-i+1}\\-(2i+1)(n-i+1)x^{i-0.5}(1-x)^{n-i}\\+(n-i+1)(n-i)x^{i+0.5}(1-x)^{n-i}\end{matrix}\right]}{i!(n-i)!}\right] \tag{18}$$

Where, x is the abscissa of airfoil points, mm; $y'(x)$ and $y''(x)$ are the first-order and second-order derivative values of the airfoil curve at each point, respectively; a_i is the shape function coefficient, namely the optimization design variable; n is the order of the shape function.

The value of the second-order derivative function is calculated for each x to determine its positivity and negativity. The amount of calculation depends on the number of two-dimensional discrete points of the airfoils, so reducing the total number of discrete points by improving the equation in the previous section can effectively decrease the amount of calculation. When the second-order derivative of the airfoil satisfies the following inequality, it can be considered that the concaveness and convexness of the airfoil profile changes once.

$$y''(x_i)\cdot y''(x_{i+1})<0 \quad i=1,2,...,n-1 \tag{19}$$

Where n is the total number of discrete points in the unilateral airfoil.

(2) Airfoil area constraints

Airfoil strength is directly related to area. Ref. [22] proves that when the main shape parameters remain unchanged, the change in airfoil area is mainly accomplished by the variation of the trailing edge profile of the lower airfoil surface, and the pressure distribution of the airfoil also varies accordingly. When the airfoil area becomes smaller, the trailing edge curve of the lower airfoil surface is concave inward. At a lower Reynolds number and a smaller flow rate, the pressure differential resistance of the airfoil increases due to the larger curved trailing edge, resulting in an increase in the force and a decrease in the strength. At the same time, the small airfoil surface area is not conducive to the setting and installation of the internal support structure of the airfoil, which also reduces the strength, and it is difficult to cooperate with other airfoils. Hence, a constraint on the airfoil area is needed. The area of the airfoil after optimization should not be less than that before optimization. The calculation formula is as follows.

$$S=\sum_{i=1}^{n}x_i\cdot[y_{\text{upper}}(x_i)-y_{\text{lower}}(x_i)] \tag{20}$$

(3) Shape-parameter constraints

According to the Refs. [23, 24], and combined with the airfoil optimization requirements in this paper, the shape parameter constraints are imposed. The $T_{\max}$ of the airfoil should be kept constant in front and behind the optimization. Considering the structural strength of the airfoil, the x_C of the optimized airfoil should be varied within a reasonable range. Therefore, the following shape parameter constraints are imposed.

$$(T_{\max})_{Optimized}=(T_{\max})_{Basic} \tag{21}$$

$$0.2\le x_C\le 0.5 \tag{22}$$

At the meantime, the optimized airfoils should have superior aerodynamic performance over a wide range of angles of attack, and the stall angle should be shifted back as much as possible. It is related to the x_T and the size of the R_{le}. For the CST parameterization method, the R_{le} is calculated as follows.

$$R_{le}=a_0^{\,2}/2 \tag{23}$$

Therefore, the following additional constraints are required.

$$0.24\le x_T\le 0.32 \tag{24}$$

$$(a_0)_{\text{Optimized}}\ge(a_0)_{\text{Basic}}. \tag{25}$$

3.3 Particle swarm optimization algorithms

This paper uses particle swarm optimization (PSO), an evolutionary computational technique based on collaboration and information sharing among individuals in a population to find the optimal solution, in combination with a neural network model for wind turbine airfoil design optimization. PSO has a simple structure, is easy to implement and requires few parameters to be adjusted.

PSO focuses on two properties of particles: position and velocity. The position is a candidate solution of the corresponding optimization problem, and the velocity corresponds to the stride size of the particle when searching in the design space. For a particle population with a certain size, each particle will randomly obtain an initial position and initial velocity, which will be updated iteratively according to Eq. (26).

$$\begin{cases} v_i = w \times v_i + c_1 \times r_1 \times (p_{\text{best}i} - x_i) + c_2 \times r_2 \times (g_{\text{best}i} - x_i) \\ x_i = x_i + v_i \end{cases} \tag{26}$$

where v is the particle velocity; x is the particle position; w is the inertia weight; c_1 and c_2 are learning factors; p_{best} is the position of individual optimal particle, that is, the particle corresponding to the historical optimal solution of a single particle; g_{best} is the position of global optimal particle, that is, the particle corresponding to the optimal solution of the whole population; r_1 and r_2 are random numbers between 0 and 1.

It can be observed that v_i in Eq. (26) consists of three parts. The first is the inertial part, which represents the tendency of the particle to maintain its previous velocity. The second is the cognition part, which reflects the memory of the particle to its own historical experience, and represents the tendency of the particle to approach to its own historical best position. The third is the social part, which reflects the group historical experience of cooperation and knowledge sharing among particles, and represents the tendency of particles to approach the historical best position of the group [25, 26]. The fitness value can be calculated according to the particle position to evaluate the merits of the solution. The fitness of the particle after updating the position is compared with the individual optimal particle and the global optimal particle. Then the above two kinds of particles are optimally updated until the maximum number of iterations or convergence is reached. Finally, the optimal solution satisfying the conditions is obtained.

3.4 Airfoil optimization process

In order to demonstrate the feasibility of the above theory, a GRNN model was established based on a small sample set. And multiple constraints were used to limit the input variables of neural network in conjunction with the actual situation of airfoil design. NACA44XX airfoil series with T_{max} of 15 %, 18 %, 21 % and 24 % were further optimized by using single-objective PSO algorithm. It took the 12-dimensional CST parameterization coefficients as design variables under specific working conditions (Re = 1.6×10^{-6}, Ma = 0.37), aiming at the maximum C_L/C_D at 5° angle of attack, to obtain a wind turbine airfoil series with better performance. The specific optimization process is as follows.

(1) Set the basic parameters. According to the number of design variables, the particle dimension was determined as 12. When the population size was set to 80, a large population can avoid the algorithm from falling into local optimum, and improve the particle search accuracy and optimization efficiency. The maximum number of iterations was 100. Adaptive learning factors and inertia weights were used, and their calculation formula is as follows [27, 28].

$$\begin{cases} w = (w_{\text{ini}} - w_{\text{end}}) \times (I_{\max} - i) / I_{\max} + w_{\text{end}} \\ c_1 = c_{\min} + (c_{\max} - c_{\min}) \times (i / I_{\max}) \\ c_2 = c_{\max} - (c_{\max} - c_{\min}) \times (i / I_{\max}) \end{cases} \tag{27}$$

Where, i is the number of current iterations, $I_{\max}$ is the maximum number of iterations, $c_{\min}$ and $c_{\max}$ are the extreme values of learning factors, w_{ini} and w_{end} are the initial and end values of inertia weight. With reference to Ref. [27], w_{ini} and w_{end} were set at 0.9 and 0.4, respectively. In the early stage of optimization, w is large and particles search the whole space at a faster speed. In the later stage, w is small to improve the local search ability. According to Ref. [28], $c_{\min}$ and $c_{\max}$ are 0.9 and 2.4, respectively. In the early stage, c_1 is smaller and c_2 is larger to maintain population diversity and avoid local optimality. In the later stage, the two are reversed to improve the convergence speed of optimization.

(2) Determine the range of design variables. The optimized airfoil thicknesses are 15 %, 18 %, 21 %, and 24 %, respectively. Using the CST parameterization coefficients of the airfoils with T_{max} equal to or close to these four thicknesses in the sample library as the boundary values, the four design variable ranges were initially obtained by taking the concatenation sets.

(3) Initialize populations. The particles were initialized randomly in the range of design variables with thickness as a constraint. To improve the computational efficiency, the CST parameterization coefficients of NACA4415, NACA4418, NACA 4421, and NACA4424 were passed into the optimization model as a set of initial particles, respectively. And, the initial fitness value corresponding to each particle was calculated.

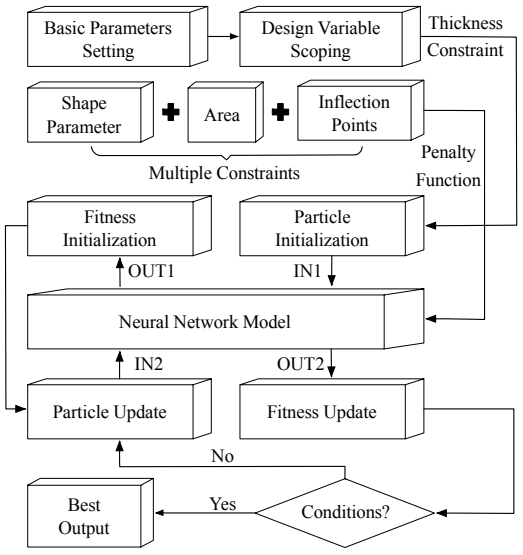

Fig. 7. Flow chart of airfoil optimization.

(4) Update and iterate. With the maximum C_L/C_D as the objective function, the fitness value was calculated by the neural network model. The profile constraints on concavity and convexity, airfoil area constraints, and shape-parameter constraints were incorporated into the fitness function in the form of penalty function. The velocity and position of the particles were continuously updated and the optimization was iterated until the best fitness was achieved. The flow chart of airfoil optimization is shown in Fig. 7.

4. Results and discussions

The iterative convergence results of particle swarm optimization algorithm are shown in Fig. 8. The fitness values of the four airfoils with different thickness converged to 136.8, 109.9, 83.9 and 53.6 after 64, 61, 53 and 80 iterations, respectively.

By substituting the global optimal particle as coefficient vector back into the CST parameterization equation, the two-dimensional discrete point coordinates of the optimized airfoils can be obtained. The shape parameters of the optimized airfoils with four thicknesses are shown in Table 2. Compared to the basic airfoils of the NACA44XX series, the C_{max} of the four optimized airfoils is increased. The x_C of the optimized airfoil with 15 % thickness moves backward, while the x_T remains unchanged. For optimized airfoils with T_{max} of 18 % and 21 % respectively, the positions of C_{max} and T_{max} move forward. The x_C of the optimized airfoil with 24 % thickness is slightly shifted back and the x_T remains the same. Fig. 9 shows the comparison of the airfoils prior to optimization and after optimization.

To verify the effectiveness of multiple constraints, an airfoil with 15 % thickness was taken as an example and optimized under different constraints, as shown in Fig. 10. Airfoil-1, airfoil-2, and airfoil-3 are the optimization results of only shape-parameter constraint, shape-parameter constraint with area constraint, and shape-parameter constraint with profile constraint, respectively. Optimized-15 % is the optimization result under multiple constraints. The coordinate data of four airfoils were imported into XFOIL. Under the condition of *Re* =

Table 2. Shape parameters of optimized airfoil with different thickness.

Optimized airfoils	C_{max}/%	x_C/%	T_{max}/%	x_T/%
Optimized-15 %	4.31	43.5	15.09	30.4
Optimized-18 %	4.57	37.3	18.09	28.6
Optimized-21 %	4.99	33.4	21.10	28.7
Optimized-24 %	5.02	40.5	24.10	30.1

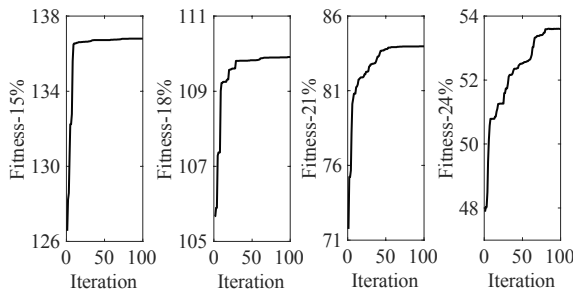

Fig. 8. Iterative process of particle swarm.

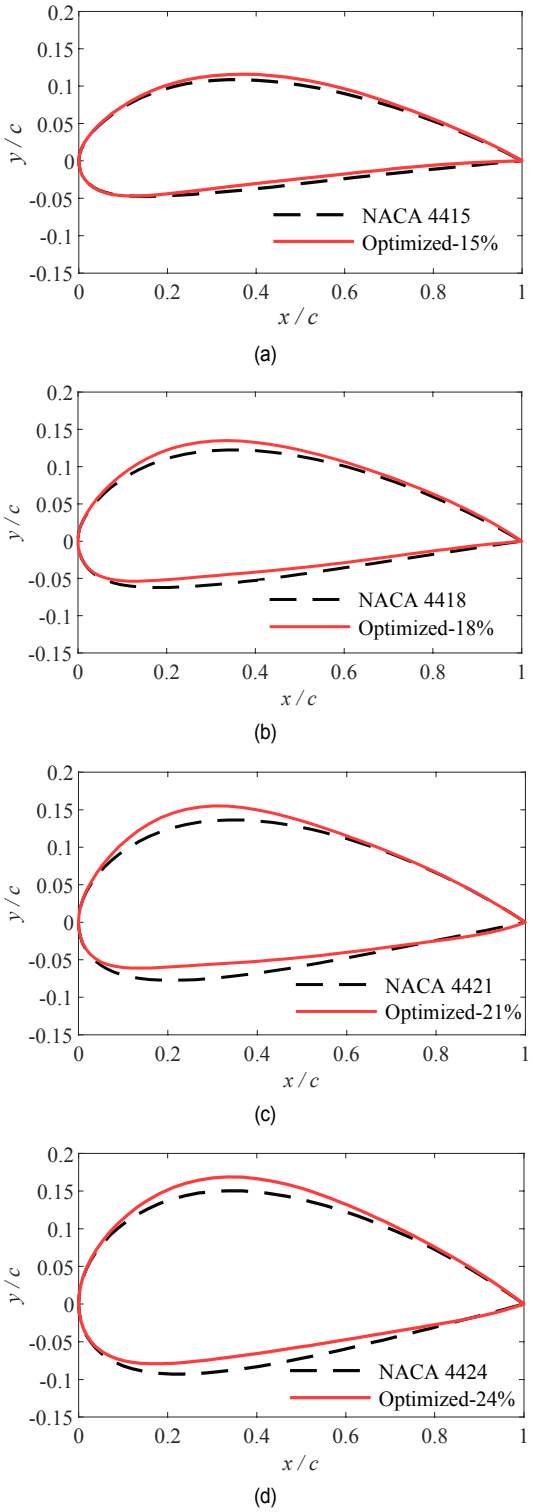

Fig. 9. Shape comparison between basic and optimized airfoil.

Table 3. Comparison of prediction errors under different constraints.

Airfoil	Angle of attack/°	Calculated C_L/C_D	Predicted C_L/C_D	Prediction error/%
Optimized-15 %	5	137.6	136.8	0.59
Airfoil-1	5	128.7	145.9	13.36
Airfoil-2	5	121.0	142.3	17.60
Airfoil-3	5	124.2	137.1	10.38

Table 4. Comparison of prediction errors for optimized airfoils with different thicknesses.

Airfoil	Angle of attack/°	Predicted C_L/C_D	Calculated C_L/C_D	Prediction error/%
Optimized-15 %	5	136.7978	137.6117	0.5914
Optimized-18 %	5	109.9128	110.3496	0.3958
Optimized-21 %	5	83.9753	83.5045	0.5638
Optimized-24 %	5	53.6070	54.0551	0.8290

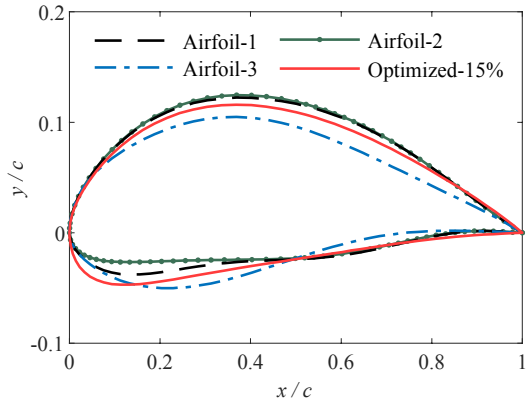

Fig. 10. Comparison of optimized airfoil shapes under different constraints.

1600000 and *Ma* = 0.37, their C_L/C_D at 5° angle of attack was calculated and compared with the predicted value of neural network. The prediction error was shown in Table 3. The error between the predicted value and the calculated value of the neural network is the smallest, only 0.59 %. The optimization effect is better, so multi-constraint conditions can be considered to be effective.

Meanwhile, the C_L/C_D of four optimized airfoils at 5° angle of attack was calculated and compared with the predicted value of neural network under the same working conditions, as shown in Table 4. The prediction errors of the four optimized airfoils are all less than 1 %, which indicates that the optimization results have high reliability.

The aerodynamic performance of basic airfoils and optimized airfoils were compared by XFOIL. When *Re* = 1600000 and *Ma* = 0.37, the aerodynamic characteristics of four airfoils with different thicknesses are analyzed at the angle of attack from 0° to 20°, and the following results are obtained.

Fig. 11 shows the comparison of aerodynamic characteristics before and after optimization of the airfoil with 15 % thickness. NACA4415 has a maximum C_L of 1.4412, appearing at an angle of attack of 13.9°. The maximum C_L for optimized airfoil is 1.4600, which occurs at 14.5° angle of attack. Compared with the original airfoil, the maximum C_L of the optimized airfoil is increased by 1.30 %, and the stall angle of attack is shifted back. In the range of 0-10° angle of attack, the C_L of the optimized airfoil is greatly improved compared with the original airfoil, with the maximum increase of 21.07 %. The maximum value of C_L/C_D for the NACA4415 is 126.06, with an optimum angle of attack of 4.7°. The optimized airfoil has a maximum C_L/C_D of 138.54, which also occurs at 4.7°. Compared with the original airfoil, the maximum C_L/C_D of the optimized airfoil is increased by 9.90 %. Therefore, the new airfoil has better aerodynamic performance.

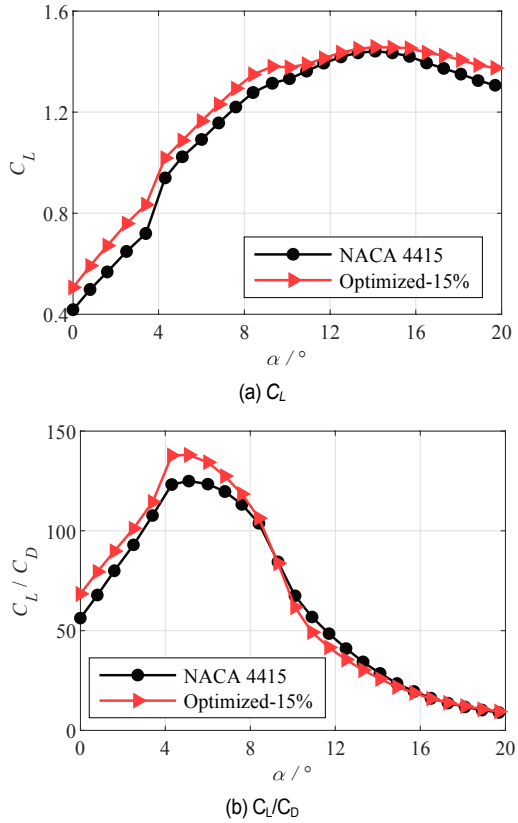

Fig. 11. Comparison of aerodynamic characteristics between basic airfoil and optimized airfoil with 15 % thickness.

The comparison of aerodynamic characteristics between basic airfoil and optimized airfoil with 18 % thickness is shown in Fig. 12. The NACA4418 has a maximum C_L of 1.4254, appearing at an angle of attack of 13°. Compared with NACA4418, the C_L of the optimized airfoil is greatly improved. Its maximum C_L is 1.6273, the lift range is 14.16 %, and the best angle of attack is 12.9°. The optimized airfoil consistently outperforms the basic airfoil in the 0-15° angle of attack. In terms of C_L/C_D, the maximum value of NACA4418 is 107.59, which occurs at 5.7°. The maximum value of the optimized airfoil is 111.32, appearing at 5.6°, which is 3.47 % higher than the original airfoil. Within 6° angle of attack, the C_L/C_D of the new airfoil is

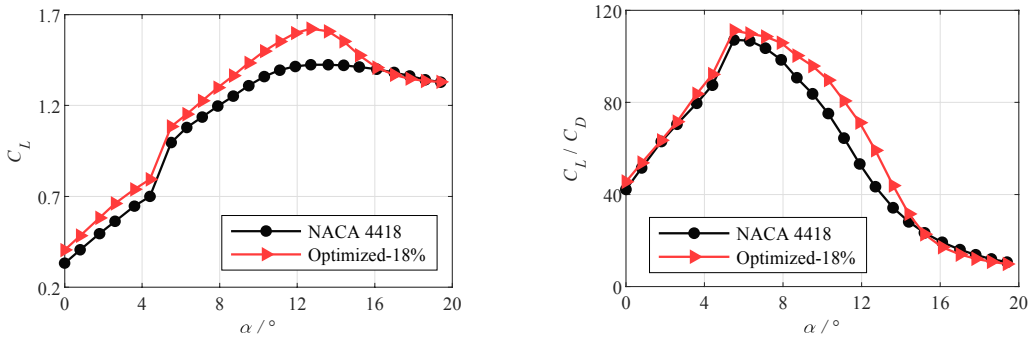

(a) C_L (b) C_L/C_D

Fig. 12. Comparison of aerodynamic characteristics between basic airfoil and optimized airfoil with 18 % thickness.

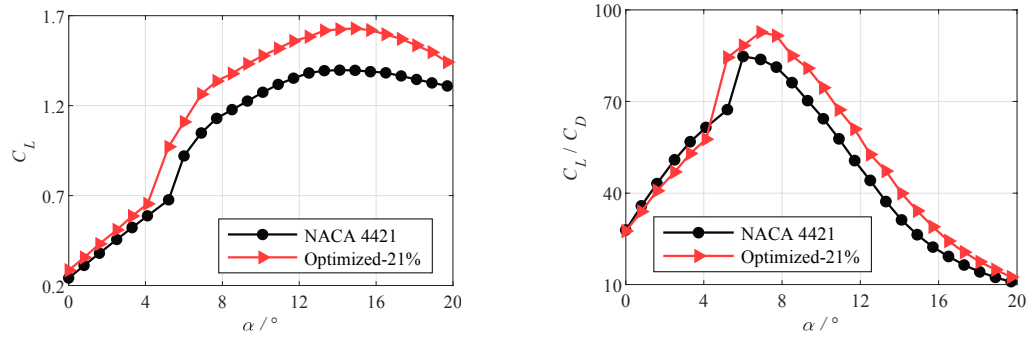

(a) C_L (b) C_L/C_D

Fig. 13. Comparison of aerodynamic characteristics between basic airfoil and optimized airfoil with 21 % thickness.

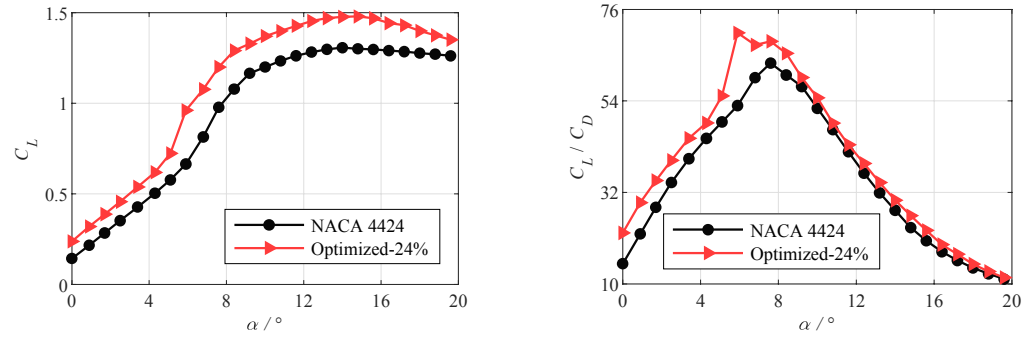

(a) C_L (b) C_L/C_D

Fig. 14. Comparison of aerodynamic characteristics between basic airfoil and optimized airfoil with 24 % thickness.

similar to that of the original airfoil, but at 6-14° angle of attack, the C_L/C_D of the optimized airfoil is much higher than that of the original airfoil.

For the airfoil with T_{max} of 21 %, the C_L is increased from 1.3985 to 1.6352 after optimization, with an improvement of 16.93 %. Stall angle of attack moved back from 14.2° to 14.5°. The C_L of the optimized airfoil is always better than that of the basic airfoil in the whole calculated angle of attack. The maximum C_L/C_D of the optimized airfoil is increased from 85.21 to 93.79, which is 10.07 % higher than that of the original airfoil. The optimal angle of attack is 7.1°. Moreover, when the angle of attack exceeds 4°, the C_L/C_D of the optimized airfoil increases more significantly, as shown in Fig. 13.

The NACA4424 is typically placed near the middle of the blade to improve structural strength by increasing thickness, but this also sacrifices part of the aerodynamic performance. The maximum C_L of NACA4424 is 1.3070 and the maximum C_L/C_D is 63.88, which is relatively poor compared to a thin airfoil. Through optimization, the new airfoil has a maximum C_L of 1.4799 at 14.2° angle of attack, a maximum C_L/C_D of 70.53, and an optimum angle of attack of 5.8°, which are superior by 13.23 % and 10.41 %, respectively. The C_L of the optimized airfoil is always better than that of NACA4424, as shown in Fig. 14. In general, the new airfoil obtained after optimization has a

large enhancement in aerodynamic performance, especially in the range of 0-8° angle of attack.

Finally, the calculation times for optimizing four airfoils with different thickness using the above method were recorded, which are 62.4443 s, 62.2643 s, 62.3087 s and 64.0657 s, respectively. The optimization time was no more than 70 seconds, which was greatly shortened compared with using XFOIL program or CFD methods. Therefore, the method can achieve rapid optimization of wind turbine airfoil design while ensuring prediction accuracy.

5. Conclusions

1) NACA four-digit airfoil equations are improved by adding an additional expression of airfoil discrete points. The validity of the improved formula is verified, which can achieve a more reasonable and accurate description of airfoil while reducing the number of points, and effectively reduce the amount of calculation in the later optimization.

2) A generalized regression neural network model is established based on small sample sets. The limitations of applying the small sample set neural network model for airfoil aerodynamic optimization design are analyzed, and multiple constraints on the airfoil design variables are proposed in a targeted manner. Optimization by multi-constraint conditions can avoid the appearance of misaligned curves and improve the accuracy of neural network model prediction.

3) Based on the small-sample neural network model under multi-constraints, the optimized design of the airfoil series was combined with the particle swarm optimization algorithm, and the new airfoils with Tmax of 15 %, 18 %, 21 %, and 24 % were obtained. Compared with the basic airfoils, the maximum C_L of the optimized airfoil increased by 1.30 %, 14.16 %, 16.93 % and 13.23 %, and the maximum C_L/C_D increased by 9.90 %, 3.47 %, 10.07 % and 10.41 %, respectively, with significant improvement in aerodynamic performance. Moreover, the optimization efficiency of this method is much higher than that of traditional methods. Therefore, the effectiveness of the method is verified.

Acknowledgements

This work is supported by the Chongqing Foundation and Frontier Project (Grant No. cstc2016jcyjA0448), Chongqing Municipal Education Commission Scientific Research Project (Grant No. KJ1600628) and Manufacturing Equipment Mechanism Design and Control Chongqing Key Laboratory Open Fund (Grant No. 1556031).

Nomenclature

C_{max} : Maximum relative camber
T_{max} : Maximum relative thickness
x_C : Maximum relative camber position
x_T : Maximum relative thickness position
R_{le} : Leading edge radius
Re : Reynolds number
Ma : Mach number
C_L : Lift coefficient
C_D : Drag coefficient
C_L/C_D : Lift-drag ratio

References

[1] M. G. Fernandez, C. Park, N. H. Kim and R. T. Haftka, Issues in deciding whether to use multifidelity surrogates, *AIAA Journal*, 57 (5) (2019) 2039-2054.

[2] C. Park, R. T. Haftka and N. H. Kim, Remarks on multi-fidelity surrogates, *Structural and Multidisciplinary Optimization*, 55 (3) (2017) 1029-1050.

[3] L. Y. Zhu, W. W. Zhang, J. Q. Kou and Y. L. Yi, Machine learning methods for turbulence modeling in subsonic flows around airfoils, *Physics of Fluids*, 31 (1) (2019) 015105.

[4] F. G. Oztiryaki and T. Piskin, Airfoil performance analysis using shallow neural networks, *AIAA Scitech 2021 Forum* (2021) 0174.

[5] J. N. Kutz, Deep learning in fluid dynamics, *Journal of Fluid Mechanics*, 814 (2017) 1-4.

[6] J. Ling, A. Kurzawski and J. Templeton, Reynolds averaged turbulence modelling using deep neural networks with embedded invariance, *Journal of Fluid Mechanics*, 807 (2016) 155-166.

[7] R. Zahn and C. Breitsamter, Airfoil buffet aerodynamics at plunge and pitch excitation based on long short-term memory neural network prediction, *CEAS Aeronautical Journal* (2021) 1-11.

[8] K. Balla, R. Sevilla, O. Hassan and K. Morgan, An application of neural networks to the prediction of aerodynamic coefficients of aerofoils and wings, *Applied Mathematical Modelling*, 96 (2021) 456-479.

[9] L. Deng, Y. Q. Wang, Y. Liu, F. Wang, S. K. Li and J. Liu, A CNN-based vortex identification method, *Journal of Visualization*, 22 (1) (2019) 65-78.

[10] V. Sekar, Q. Jiang, C. Shu and B. C. Khoo, Fast flow field prediction over airfoils using deep learning approach, *Physics of Fluids*, 31 (5) (2019) 057103.

[11] W. L. Lyu, S. Y. Wang and A. M. Yang, Some improvements of hybrid trim method for a helicopter rotor in forward flight, *Aerospace Science and Technology*, 113 (2021) 106709.

[12] Y. J. Sun, G. Sun and S. Y. Wang, Neural net based wing shape prediction, *Chinese Quarterly of Mechanics*, 35 (3) (2014) 482-490.

[13] X. Y. Wang, S. Y. Wang, J. Tao, G. Sun and J. Mao, A PCA–ANN-based inverse design model of stall lift robustness for high-lift device, *Aerospace Science and Technology*, 81 (2018) 272-283.

[14] A. Kharal and A. Saleem, Neural networks based airfoil generation for a given cp using bezier-parsec parameterization, *Aerospace Science and Technology*, 23 (1) (2012) 330-344.

[15] Y. F. Zhang, C. Y. Yan and H. X. Chen, An inverse design method for airfoils based on pressure gradient distribution, *En-*

ergies, 13 (13) (2020) 3400.

[16] H. P. Wang, X. Jiang, Y. Chao, Q. Li, M. Z. Li, T. Chen and W. R. Ouyang, Numerical optimization of horizontal-axis wind turbine blades with surrogate model, *Proceedings of the Institution of Mechanical Engineers, Part A: Journal of Power and Energy,* 235 (5) (2021) 1173-1186.

[17] A. J. Al-Mahasneh, S. G. Anavatti and M. A. Garratt, Evolving general regression neural networks for learning from noisy datasets, *2019 IEEE Symposium Series on Computational Intelligence (SSCI)*, Xiamen, China (2019) 1473-1478.

[18] F. R. Marzabadi, M. Masdari and M. R. Soltani, Application of artificial neural network in aerodynamic coefficient prediction of subducted airfoil, *Journal of Research in Science and Engineering*, 2 (1) (2020) 13-17.

[19] J. E. Stolzman and S. Manoharan, Testing the efficacy of dimples on a naca airfoil at low Reynolds numbers: a numerical study, *AIAA Aviation 2021 Forum* (2021) 2584.

[20] Z. H. Han, Kriging surrogate model and its application to design optimization: a review of re-cent progress, *Acta Aeronautica et Astronautica Sinica*, 37 (11) (2016) 3197-3225.

[21] X. C. Sun, Z. H. Han, F. Liu, K. Song and W. P. Song, Design and analysis of hypersonic vehicle airfoil/wing at wide-range mach numbers, *Acta Aeronautica et Astronautica Sinica*, 39 (6) (2018) 31-42.

[22] R. F. Xu, W. P. Song and K. Zhang, Investigation of effect of transition on wind turbine airfoil optimization design, *Acta Energiae Solaris Sinica*, 32 (12) (2011) 1798-1803.

[23] J. Chen, Q. Wang, S. L. Li, X. F. Guo and X. D. Wang, Study of optimization design method for wind turbine airfoil combining airfoil integrated theory and B-spine, *Acta Energiae Solaris Sinica*, 35 (10) (2014) 1930-1935.

[24] J. Chen, Q. F. Lu, X. D. Wang and J. T. Cheng, Research on optimization of general airfoil profiles for wind turbines based on adaptive genetic algorithm, *China Mechanical Engineering*, 20 (20) (2009) 2448-2451+2469.

[25] F. Q. Miao, H. S. Park, C. Kim and S. Ahn, Swarm intelligence based on modified PSO algorithm for the optimization of axial-flow pump impeller, *Journal of Mechanical Science and Technology*, 29 (11) (2015) 4867-4876.

[26] T. Deshamukhya, D. Bhanja, S. Nath and S. A. Hazarika, Prediction of optimum design variables for maximum heat transfer through a rectangular porous fin using particle swarm optimization, *Journal of Mechanical Science and Technology*, 32 (9) (2018) 4495-4502.

[27] Y. Shi and R. Eberhart, Empirical study of particle swarm optimization, *Proceedings of the 1999 Congress on Evolutionary Computation*, Washingdon, DC, USA (1999) 1945-1950.

[28] Z. H. Zhan and J. Zhang, Adaptive particle swarm optimization, *IEEE Transactions on System, Man, and Cyber-netics-Part B*, 39 (6) (2009) 1362-1381.

Xudong Wang is a Professor at Chongqing Technology and Business University. He received his Ph.D. degree in Mechanical Design and Theory from Chongqing University, Chongqing, in Jun. 2009. From Sep. 2007 to Sep. 2008, he was a Joint Training Ph.D student with the School of Mechanical Engineering, the Technical University of Denmark. His research interests include dynamics of Machinery, optimization design and intelligent Vehicles.